Bioactive glass containing silicone composites for left ventricular assist device drivelines: role of Bioglass 45S5® particle size on mechanical properties and cytocompatibility

Journal Article

Author(s):
Cohrs, Nicholas H.; Schulz-Schönhagen, Konstantin (ID); Jenny, Florian; Mohn, Dirk; Stark, Wendelin J.

In Honor of Larry Hench

CrossMark

Bioactive glass containing silicone composites for left ventricular assist device drivelines: role of Bioglass 45S5® particle size on mechanical properties and cytocompatibility

Nicholas H. Cohrs[1], Konstantin Schulz-Schönhagen[1], Florian Jenny[1], Dirk Mohn[1,2], and Wendelin J. Stark[1,*]

[1] Department of Chemistry and Applied Biosciences, Institute for Chemical- and Bioengineering, ETH Zurich, Vladimir-Prelog-Weg 1, 8093 Zurich, Switzerland

[2] Clinic of Preventive Dentistry, Periodontology and Cariology, Center of Dental Medicine, University of Zurich, Zurich, Switzerland

ABSTRACT

Aside its historical use in contact with bone and teeth, an increasing number of studies use bioactive glasses (BG) in contact with soft tissue. BG could provide solutions for various medical problems. This study presents a first evaluation, whether BG containing silicone elastomers are a suitable material for left ventricular assist device drivelines and could enhance skin biointegration thereof. Three different nano- or microparticles of BG45S5® were incorporated into medical grade silicone elastomer, and thin films of the composites were manufactured. Physicochemical, mechanical and in vitro experiments using primary human dermal fibroblasts were used to evaluate the nano- and microcomposites. The incorporation of BG particles reduced the tensile strength at break and percent elongation at break of the composites and increased the stiffness of the material. Especially, the incorporation of nanosized BG decreased the percent elongation at break after immersion in SBF due to agglomerate formation and increased hydroxyapatite formation compared to commercially available microparticles. The cytocompatibility of BG containing composites increased significantly with increasing particle concentration. A clear trend regarding particle size was not observed. In general, the simple incorporation of particles into medical grade silicone elastomer allowed an easy modification of the mechanical properties and improvement in bioactivity (assessed by hydroxyapatite formation) of the material. The choice of either nano- or microparticles depends on the specific application and requirements for the material, as different particle types show different advantages and disadvantages.

Address correspondence to E-mail: wstark@ethz.ch

Springer

Introduction

Bioactive glass (BG) is an amorphous material, which consists of a combination of various oxides. Its classical and best known composition is BG45S5®, described by Hench et al. in 1971 with a composition of 45 wt% SiO_2, 24.5 wt% Na_2O, 24.5 wt% CaO and 6 wt% P_2O_5 [1–3]. Its properties such as bioactivity, osteoconductivity and osteostimulation make BG a suitable material in contact with hard tissue such as bone and teeth [4]. The bioactive properties of BG result from its reaction with the body fluids to form a direct bond with bone [1, 2]. Also, its leaching in body fluids causes a change in the local ionic environment, which stimulates osteoblast proliferation, increases angiogenesis and acts antibacterial [5–10].

Besides the use of BG with hard tissue, an increasing number of studies used BG in contact with soft tissue. Miguez-Pacheco et al. [8] have presented a thorough literature review on this topic. They reported multiple studies, which showed that "BG can have a stimulatory effect on angiogenesis, which is also applicable to soft tissue engineering" [8]. The applicability of BG for cardiac tissue engineering, wound healing and dressing, nerve regeneration, gastrointestinal regeneration, urinary tract and lung tissue engineering, laryngeal repair and stabilization of percutaneous devices is also reported [11–22].

The combination of the aforementioned and well-known properties of BG and the recently reported findings could provide further possible solutions for other medical problems. Issues are, for example, faced in heart surgery and in more detail in heart replacement therapy. An increasing number of left ventricular assist devices (LVADs) are implanted into patients with heart failure every year, reaching 5000 devices in 2015 [23]. LVADs are small blood pumps, which are implanted into the body and support the weakened heart. These implants are either driven electrically or pneumatically, which requires a percutaneous lead, the so called driveline, which connects the power source with the implanted LVAD in the body. The situation is sketched in Fig. 1. The driveline exit site (DLES) is the place, where the lead exits the patient and is considered as the "Achilles heel" of LVADs [23]. It is most susceptible to infection and constitutes as an entry point for germs [24]. In one of the trials for the HeartMate II, a currently

frequently implanted LVAD, an infection rate of 37% per patient-year was reported [23, 25].

The LVAD drivelines are approximately 95 cm long and partly covered with a polyethylene terephthalate or polyester velour (Dacron® velour) with a length of approximately 30 cm [26]. The velour is used, because it offers reasonable epidermal biointegration [27]. In the past, the velour was placed at the driveline exit site, with an externalized part of approximately 2 cm (Fig. 1a), because it was believed to promote tissue ingrowth and thus optimize the driveline stability at the driveline exit site [24, 26]. However, cardiac surgeons started to put the smooth silicone or polyurethane surface of the leads itself at the position of the driveline exit site due to seemingly reduced infection rates and faster skin incorporation, thus internalizing the entire velour-covered portion of the driveline (Fig. 1b) [23, 28, 29]. The reason for these better patient outcomes is believed to be less dermal inflammation of the polymer–skin interface, compared to a velour–skin interface, thus yielding faster incorporation of the skin [30]. However, infections still occur very frequently [24]. The main reason for infections with a polymer–skin interface is believed to be trauma at the driveline exit site, disrupting the integrity of the driveline–skin barrier and thus, giving an entry point for germs [24]. Therefore, a long-term stable connection of skin with the driveline's material, e.g. silicone, giving mechanical stability between the polymer and skin, is desirable.

Ross et al. (2003) tackled a similar problem. They used microscale particles of BG45S5® to coat a peritoneal dialysis catheter and studied its influence on tissue ingrowth by implanting the coated silicone catheters subcutaneously in a rat model [20, 21]. They showed that the BG coated tubes were "palpably fixed to the soft tissue", while the uncoated control did not result in a stable tissue–silicone interface [21]. This concept of using bioactive glass on the surface of percutaneous devices could also be applied to percutaneously implanted drivelines of LVADs, in order to allow a faster formation and more stable polymer–skin interface, thus giving improved mechanical stability and a long-term stable barrier against pathogens.

To study the influence of BG45S5® particles on silicone elastomers, different BG particles were incorporated into medical grade silicone. It is of significant interest, whether the incorporation of these bioactive particles into the silicone elastomer

influence their mechanical properties. Further in vitro tests using simulated body fluid and cell culture tests with human primary dermal fibroblasts were used for a first assessment, whether the material could be suitable for skin biointegration. We therefore investigated, whether the incorporation of different BG45S5® particles in medical grade silicone elastomers improves the mechanical properties, the bioactivity and cytocompatibility of silicone elastomers. These experiments provide a first approximation, if BG containing silicone could be used and if it could improve the polymer–skin interface of percutaneous devices, especially at the driveline exit site of LVAD drivelines.

Materials and methods

Production of the bioactive glass containing films

Nanoscale bioactive glass particles (nano-BG) of the type 45S5® were produced using flame spray synthesis as described earlier by Brunner et al. [31]. Briefly, the corresponding amounts of precursors (based on Si, Na, Ca and P) were mixed and diluted with tetrahydrofuran (THF, inhibitor-free, Sigma-Aldrich, Buchs, Switzerland) at a volumetric ratio of 2:1. The mixture was dispersed in oxygen and ignited in a methane and oxygen flame. The nanoparticles

were collected on a filter and sieved subsequently. The commercially available microscale particles were provided by Schott (Schott-BG, bioactive glass 45S5®, SCHOTT, Landshut, Germany) and mo-Science (Mo-Sci-BG, 45S5® Bioactive Powder, Mo-Sci Health Care LLC, Rolla MO, USA). Schott-BG has a primary particle size of 4 μm, and Mo-Sci-BG has a primary particle size of ≤54 μm, as specified by the suppliers. The silicone elastomer films with the specific BG content (Table 1) were produced by blending particles into a 2-component addition cure medical grade silicone elastomer (silicone, Silicone Elastomer A-103, Factor II Inc., Lakeside AZ, USA), which is cured by a platinum catalyst. According to the supplier, the platinum catalyst was included in component A. In detail, the corresponding amounts of silicone component A and BG particles were mixed in a dual-axis centrifuge (Speed Mixer DAC 150 FVZ, Hausschild Engineering, Hamm, Germany) for 2 min at 3500 rounds per minute (rpm). Afterwards, vacuum was applied to 8 mbar for approximately 5 min. For each sample, this procedure was repeated 4 times. Afterwards, the corresponding amount of silicone component B was added and again mixed for 2 min at 3500 rpm. The uncured BG-silicone mixture was degassed to 8 mbar for approximately 10 min. The films were prepared using an automatic film applicator (Elcometer 4340, 120 μm rakle, Elcometer Instruments GmbH, Germany) on aluminium sheets, which had been washed with ethanol (EtOH, puriss.
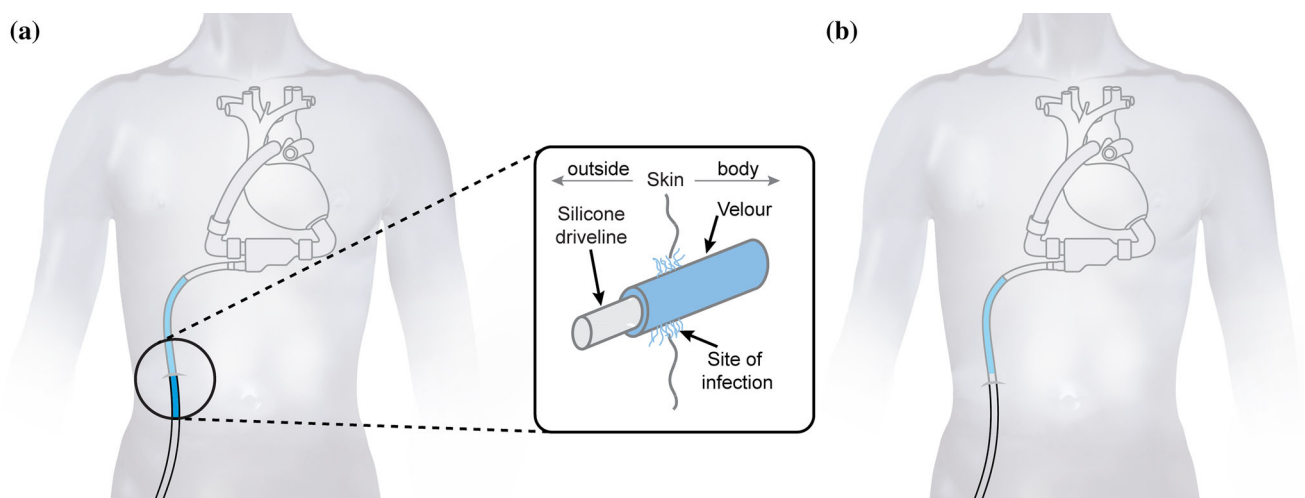

Figure 1 Sketch of the surgical technique of implanting the driveline of a left ventricular assist device. In **a,** the velour is placed at the driveline exit site yielding a velour–skin interface. **b** Shows an implanted driveline with a polymer–skin interface at the driveline exit site. In this case, the velour portion of the driveline is completely internalized inside the patient's body. With the courtesy of Berlin Heart GmbH.

Table 1 Silicone composites with different bioactive glass (BG) loadings and types

Particle type primary particle diameter (µm)[a]	Control	Nano-BG 0.02–0.06	Schott-BG 4	Mo-Sci-BG ≤54
Concentrations (wt%)	0	5 10[b]	5 10 15	5 10 15

[a] As specified by supplier or literature [31]

[b] 15 wt% nano-BG could not be manufactured

p.a., Sigma-Aldrich) before. Subsequently, the films were cured at 150 °C in an oven for 6 h.

Characterization of the materials

Characterization of Bioglass 45S5® particles

BG45S5® particles were analysed by scanning electron microscopy (SEM, FEI NovaNanoSEM450, FEI, Eindhoven, The Netherlands). Prior to SEM, the samples were sputtered with a 5 nm layer of platinum. The particle size distribution (PSD) was measured by analysing the size of at least 300 particles in a random area for each sample. The diameter of the particles was determined using an ellipse to fit the particles' outlines and taking the average of the major axis and the minor axis as the approximate diameter of each particle.

In vitro tests using simulated body fluid and analysis of bioactive glass containing films

The in vitro bioactivity of BG containing films was tested in simulated body fluid (SBF). SBF was prepared according to Kokubo and Takadama with a pH of 7.4 [32]. Films were cut (100×20 mm) and washed in ethanol, dried in vacuum overnight and weighed ($M_{0,dry}$). Afterwards, each sample was incubated in 45 mL of freshly prepared SBF in a water bath at 36.5 °C for 4 weeks, and SBF was replaced once a week. After incubation, the samples were gently dried on paper, weighed ($M_{t,wet}$) and afterwards dried in vacuum for 1 week. Dried samples were weighed ($M_{t,dry}$) to determine the weight loss (%WL) and water uptake (%WA) [33], which were calculated according to

$$\%\text{WL} = \left(\frac{M_{0,dry} - M_{t,dry}}{M_{0,dry}}\right) \times 100$$

$$\%\text{WA} = \left(\frac{M_{t,wet} - M_{t,dry}}{M_{t,dry}}\right) \times 100.$$

The formation of hydroxyapatite (HAp) of the samples was analysed by taking SEM images of the planar section as well as the cross section of all samples before and after immersion in SBF. The samples for the cross-sectional SEM images were frozen using liquid nitrogen (LN₂). Two tweezers, whose tips had also been cooled in LN₂, were used to break the film and form a break line. The films were mounted on the SEM sample holders and sputtered as described earlier. Cross-sectional SEM images were taken of this break line. Additionally, X-ray diffraction (XRD, X'Pert PRO-MPD, PANalytical, Almelo, The Netherlands) was used with Ni-filtered Cu Kα radiation ($\lambda = 0.1541$ nm) from 10° to 70° in the 2Θ scale with a step size of 0.05° at 6 s per step to confirm the presence of HAp.

Physical properties analysis

ASTM test method D882 – 12 was used to measure the influence of the different particles and concentrations on the mechanical properties of the silicone. Briefly, BG-silicone composite films were cut into rectangles (100×20 mm), and the thickness of the films was measured (Digimatic Outside Micrometer IP65, Mitutoyo, Urdorf, Switzerland) at 3 random locations on each sample to ensure a variation in thickness of less than 10%. The mechanical properties were tested of as-prepared BG-silicone films ($n \geq 4$) and BG-silicone films, which had been immersed in SBF for 4 weeks ($n \geq 3$) using a tensile tester (Shimadzu AGS-X, 10 kN load cell, Reinach, Switzerland). The gauge length was 50 mm, and the test speed was 500 mm min⁻¹. Engineering stress and engineering strain were measured, and a tangent in the linear regime of the stress–strain curve was used to calculate the Young's modulus. Measurements
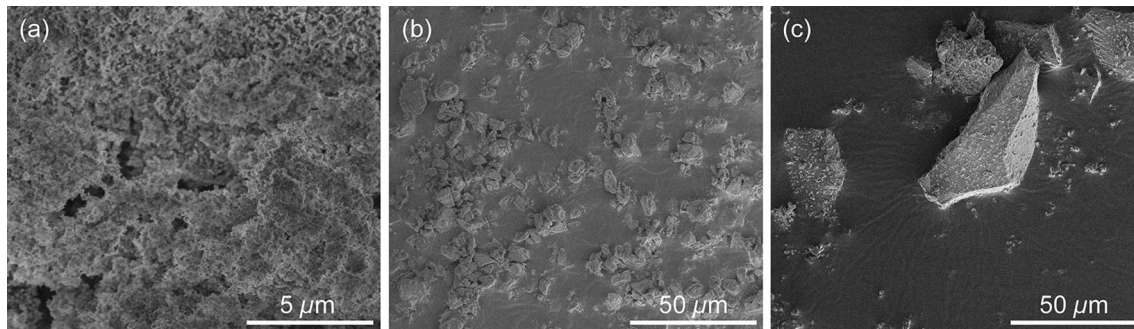
Figure 2 Scanning electron microscopy images of the different bioactive glass BG45S5® particles. **a** Nanosized bioactive glass (nano-BG), prepared by flame spray synthesis, commercial microparticles by **b** Schott (Schott-BG) and **c** Mo-Sci Corporation (Mo-Sci-BG).

were taken until failure of the material and measurements of rupture at the grip were not considered. Static contact angle measurements (NRL C, Ramé-hart Inc., Randolph NJ, USA) were taken in order to determine the hydrophobicity of the as-prepared samples. In total, 20 µL drops of deionized water were added on the surface. Every sample was analysed using three droplets. The left angle of each droplet was measured for 36 s at a rate of 25 images per second, which gave 901 measurements of the static contact angle. The average of these measurements was used to give the static contact angle of each droplet, while the average of the three droplets gave the reported value of each material.

Cell culture study

Materials

Normal Human Primary Dermal Fibroblasts from neonatal foreskin were purchased from ATCC (ATCC® PCS-201-010™, Manassas VA, USA). The cells were cultivated in Fibroblast Basal Medium (FBM, Lonza, Walkersville MD, USA) using a low serum Fibroblast Growth Medium Kit (FGM-2 SingleQuot Kit Suppl. & Growth Factors, Lonza) and incubated at 37 °C in humidified air (37 °C, 5% CO_2). Dulbecco's Phosphate Buffered Saline (DPBS (1X), gibco®, Paisley, UK) was applied to wash the cells, while Trypsin–EDTA (0.25% Trypsin–EDTA (1X), gibco®) was used for trypsinization of the cells.

Test samples and cell seeding

Uncured BG-silicone was filled into 48 well plates (Nunclon Delta Surface 48 well plate, Thermo Fischer Scientific, Waltham MA, USA), shaken orbital by

hand and cured in an oven at 40 °C for 7 days. Afterwards, the cell culture plates were disinfected with UV-C light from four low-pressure mercury lamps (253.7 nm, 15 W, HNS 15 ORF, Osram). The UV-C lamps were set at a distance of 50 cm from the sample, resulting in a dose rate of approximately 5.2 W m^{-2}. The irradiation output was measured by a standard photodiode sensor (PD300-UV, 200–1100 nm, 3 mW 20 pW, OphirPhotonics) [34]. Cells (passage #5) were seeded at a concentration of 2,500 cells cm^{-2} in 600 µL FBM and incubated at 37 °C and 5% CO_2 for up to 7 days. For every material, 12 wells were sampled, 4 for every measuring time. The medium was changed every 48 h.

Relative cell proliferation assay

Relative cell proliferation of human primary dermal fibroblasts on the different materials was measured using a commercial cell viability reagent (PrestoBlue™ Cell Viability Reagent, Invitrogen Ltd., Paisley, UK), which assesses the cell viability via the metabolic activity of the cells. The reagent was first filtered (Filtropur S 0.2, Sarstedt AG & Co., Nürnbrecht, Germany). In total, 60 µL of the filtered viability reagent were added to each well containing the different materials. For each measuring time, 4 replicates of every composite were assessed. After addition of the viability reagent, the well plate was gently shaken and incubated at 37 °C in humidified air for 2 h. Three times 100 µL of each sampled well were added to a 96-well plate (Tissue Culture Test Plate 96F, TPP®, Trasadingen, Switzerland) and analysed using fluorescence (TECAN infinite F200, Tecan Group Ltd., Männedorf, Switzerland) at an absorbance of 560 nm and emission of 590 nm at 4 different spots in every well. The cell proliferation
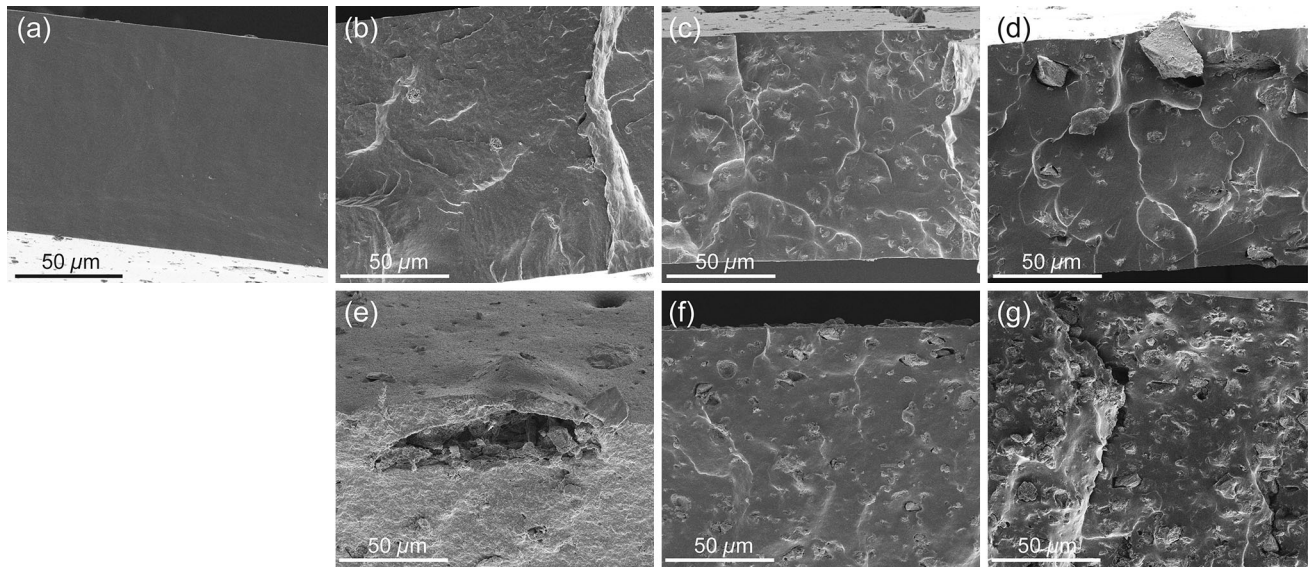
Figure 3 Cross-sectional scanning electron microscopy images of as-prepared silicones containing 10 wt% bioactive glass (BG45S5®) particles. **a** The pure silicone, **b** with nanosized bioactive glass (nano-BG), **c** with microparticles by Schott (Schott-BG) and **d** with microparticles by Mo-Sci-Corporation (Mo-Sci-BG). Figure 3e–g shows the respective particle containing composite films after 4 weeks immersed in simulated body fluid.

assay was conducted 1, 3 and 7 days after cell seeding.

Statistical analysis

Results are represented as mean ± standard deviation. The number of samples differed, but was noted, at the presentation of the results, when useful. Statistical significance was analysed using one-way analysis of variance (ANOVA) with a Bonferroni's post hoc correction (OriginPro 9.1.0, Origin Lab Corp. Northampton MA, USA). Significance of the results of the experiments was assumed at a p value of <0.05.

Results

Bioactive glass characterization

The three particle types differed in their shape and primary particle size (Fig. 2). Nano-BG appeared as spherical particles within large agglomerates, while Schott- and Mo-Sci-BG particles showed a shard-like appearance with larger primary particle sizes and sharp edges. The primary particle size of nano-BG was approximately 40 nm (Fig. S9) with agglomerates of 11.85 ± 6.10 μm. Schott- and Mo-Sci-BG particles did not seem agglomerated and had a primary particle size of 3.27 ± 1.79 μm and 10.83 ± 4.08 μm,

respectively. Schott-BG showed a lean particle size distribution (Fig. S2), while Mo-Sci-BG also consisted of larger single particles of up to 65 μm (Fig. 2c and S3).

Morphology of nano- and microcomposites

SEM images confirmed the presence of BG particles on the surface of silicone composite films (Fig. S10a–c). The large agglomerates of the nano-BG seemed to be broken up into smaller fractions. Especially, the very large and shard-like Mo-Sci-particles could be observed. Cross-sectional SEM images confirmed the evenly dispersed BG particles in the silicone composite films (Fig. 3 and S8). Agglomerates of nano-BG particles were still present as shown in Fig. 3, while also smaller, more evenly dispersed nano-BG particles could be observed. Schott-BG and Mo-Sci-BG containing films seemed to have an even dispersion of incorporated particles. More detailed cross-sectional SEM images are available in the supporting information in Fig. S8.

In vitro bioactivity study

BG containing composites exhibited HAp formation on their surfaces (Figs. 3e–g, 4c, d, Fig. S8c, e, g). Schott-BG and Mo-Sci-BG containing films showed
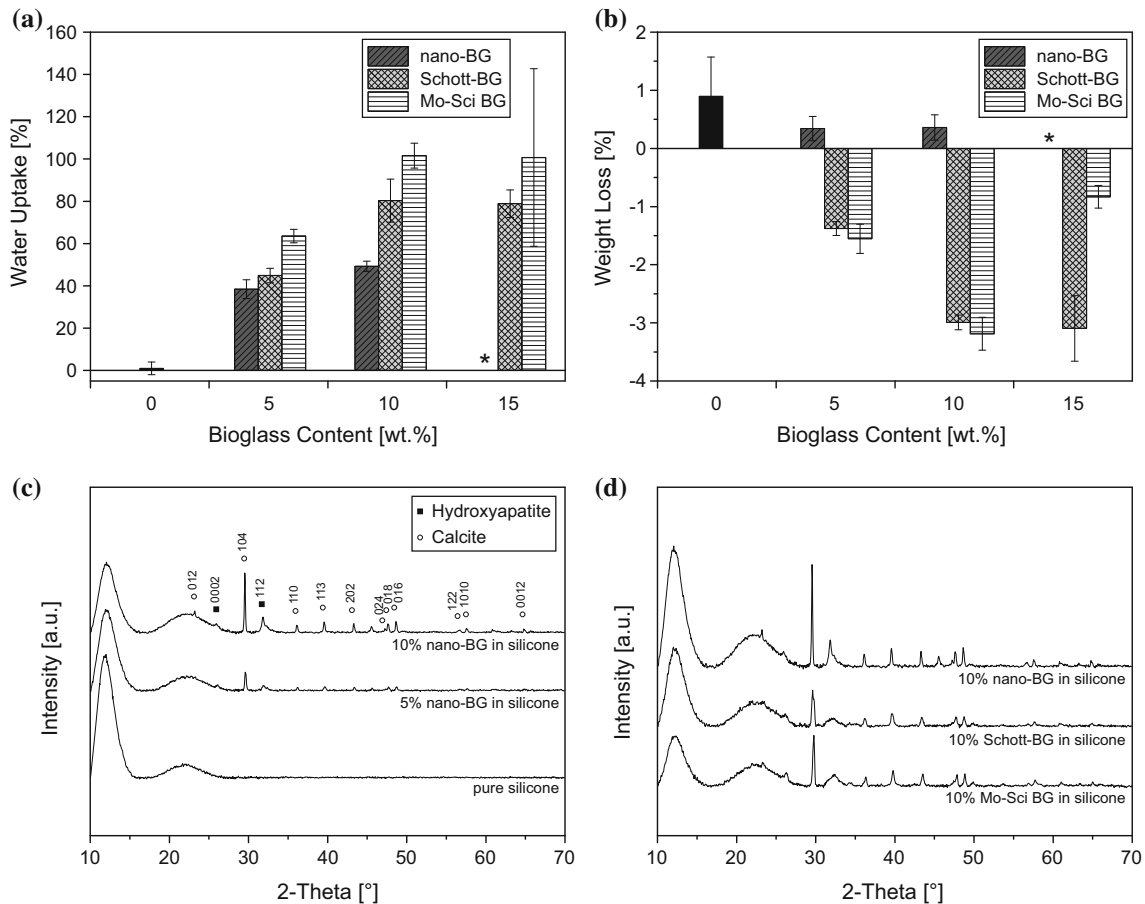
Figure 4 Surface and bulk composite changes after in vitro tests in simulated body fluid (SBF). **a** Gives the water uptake (%WA) of the wet films after 4 weeks in SBF, while **b** shows the respective weight loss (%WL) of the dry films. **c** X-ray diffractogram (XRD) of a nano-BG containing silicone film after 4 weeks in SBF and its concentration dependence; **d** illustrates the respective dependence of the particle type at a constant concentration of 10 wt%. * 15 wt% composition of nano-BG was not producible.

crater formation after 4 weeks in SBF, while HAp formed evenly on the surfaces of nano-BG containing films. Cross-sectional SEM images of the films showed that in nano-BG containing composites HAp was formed more evenly dispersed as compared to microcomposites. For Schott-BG and Mo-Sci-BG containing silicones, the HAp formation was located at the larger microparticles, which, due to their size, were not as well distributed across the silicone matrix as compared to the nanoparticles.

XRD patterns of as-prepared composites revealed the amorphous nature of pure and BG containing silicone films (Fig. 4c, d and Fig. S4-6). After immersion in SBF for 4 weeks, the characteristic signals of HAp at $2\Theta = 26°$ (0002) and $2\Theta = 31.5°$ (112) appeared. All diffractograms of BG containing films showed patterns for HAp and calcium carbonate (calcite) after immersion in SBF. The signals of the

HAp for nano-BG containing composites were sharper compared to the microparticles containing silicone composites. The area below the HAp-signals increased with increasing particle concentrations in the films and with increasing duration of immersion. Also, depending on the particle type, the integral of the HAp peaks (specifically 112) decreased from nano-BG to Mo-Sci-BG to Schott-BG, indicating the amount of measured HAp.

The water uptake increased with increasing particle concentration (Fig. 4a). It was the lowest for nano-BG and the highest for Mo-Sci-BG containing silicone films. For larger concentrations, the water uptake seemed to plateau and did not change significantly ($p = 1$) between 10 and 15 wt% Schott-BG and Mo-Sci-BG, respectively. Pure silicone films did not show any swelling behaviour. There was no significant difference in mass loss between pure and nano-BG

Table 2 Static contact angle (°) measurements of bioactive glass (BG) particle containing silicone films with different particle types and concentrations

Pure Si	5% nano-BG	10% nano-BG	5% Schott-BG	10% Schott-BG	15% Schott-BG	5% Mo-Sci-BG	10% Mo-Sci-BG	15% Mo-Sci-BG
111 ± 3	105 ± 5	107 ± 3	107 ± 1	105 ± 6	105 ± 1	108 ± 2	109 ± 3	102 ± 3

The measurements were taken in triplicates

containing films ($p = 0.68$ for blank vs. 5 wt% nano-BG, $p = 0.82$ for 10 wt% nano-BG, Fig. 4b). In contrary, the weights of the films containing larger Schott-BG and Mo-Sci-BG particles were significantly larger compared to the blank ($p \leq 2.27 \times 10^{-7}$). These weight gains increased with increasing particle concentrations and plateaued for Schott-BG composites at large concentrations ($p = 1$ for 10 wt% Schott-BG vs. 15 wt% Schott-BG), while it decreased for Mo-Sci-BG composites at 15 wt% compared to 10 wt% Mo-Sci-BG composites ($p = 2 \times 10^{-7}$).

Mechanical properties

Static contact angle

Pure silicone films showed the highest hydrophobicity and the static contact angle decreased with increasing particle concentration in the composite (Table 2). No significant difference between the materials was measured in this experiment ($p \geq 0.28$).

Tensile strength at break

The incorporation of Mo-Sci-BG microparticles decreased the tensile strength at break of the silicone films. The measurements were significant for a mass concentration of 5 wt% ($p = 0.02$), while no significant results for 10 ($p = 0.78$) and 15 wt% ($p = 1$) of Mo-Sci-BG composites could be measured compared to pure silicone, respectively. Nano-BG and Schott-BG particles did not influence the tensile strength at break of as-prepared composite films, as compared to pure silicone films ($p = 1$). The tensile strength at break was independent of the particle concentration ($p = 1$) for all particle types (Fig. 5a). After immersion in SBF for 4 weeks, the tensile strength at break was reduced for any type of composite film compared to as-prepared films (Fig. 5b). However, the results only showed a significant reduction in the tensile strength at break of 10 wt% nano-BG films

after immersion ins SBF compared to as-prepared films ($p = 0.0005$). The value for Mo-Sci-BG composites did not change significantly compared to as-prepared Mo-Sci films ($p = 1$), while the values of Schott-BG films after immersion in SBF reduced evenly and remained independent of the concentrations compared to as-prepared films.

Elongation at break

The elongation at break of the silicone composites was reduced for composites with incorporated particles (Fig. 5c). However, a significant reduction in the elongation at break was only measured between pure silicone and 5 wt% nano-BG ($p = 0.03$) and between pure silicone and 10 wt% nano-BG ($p = 0.0003$). The applied in vitro conditions did not have an influence on the elongation at break of pure silicone films ($p = 0.91$). In contrary, the elongation at break reduced after immersion in SBF in comparison with as-prepared films with increasing BG concentrations and especially for 10 wt% nano-BG containing films with $47 \pm 31\%$. Besides a significant reduction in elongation at break of nano-BG containing films (5 wt% nano-BG: $p = 0.00007$; 10 wt% nano-BG: $p = 0.000002$) after immersion in SBF, the reduction was most distinct for films containing large BG concentrations of 15 wt%, with a significant reduction in the elongation at break of the 15 wt% Mo-Sci-BG composite ($p = 0.001$) compared to the as-prepared film.

Stiffness

The Young's modulus of particle containing composites before immersion in SBF increased with increasing particle concentrations, while it decreased with increasing particle size (Fig. 5e). Specifically, nano-BG containing composites were stiffer with increasing particle composition ($p < 2 \times 10^{-22}$), but also Schott-BG composites and Mo-Sci-BG composites were stiffer with increasing particle composition compared to pure silicone. There was no significant
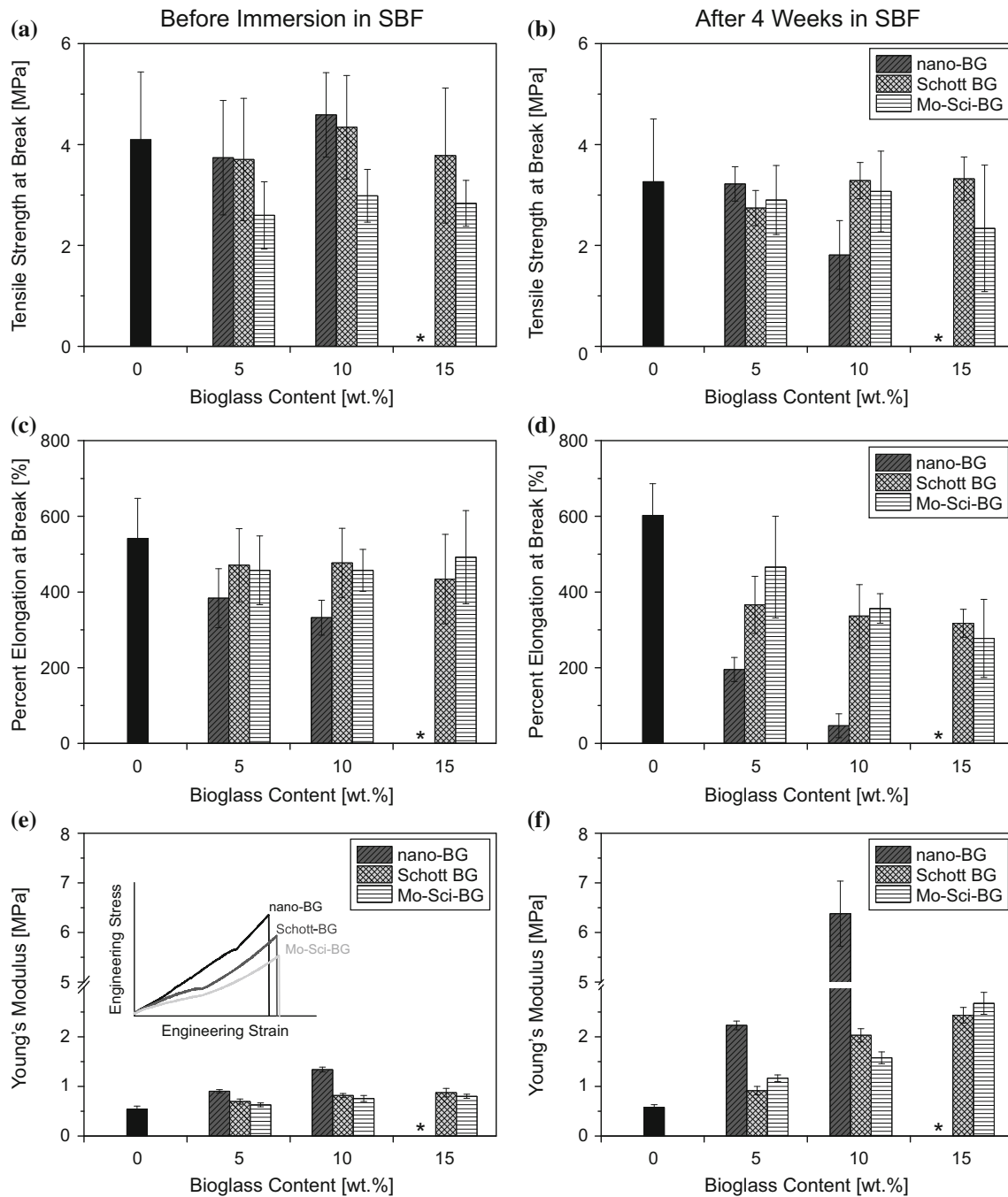
Figure 5 Influence of different bioactive glass (BG45S5®) particles and particle concentrations in silicone films on the mechanical properties of the composite. **a** Gives the tensile strength at break of the as-prepared silicone films as a function of concentration and particle type, while **b** gives the respective values, after immersion in simulated body fluid (SBF). **c** Shows the percent elongation at break of the as-prepared films and **d** depicts the value after immersion in SBF for 4 weeks. **e** and **f** Represent the Young's modulus of the films before and after immersion in SBF. * 15 wt% composition of nano-BG was not producible **e** also contains typical stress–strain curves of as-prepared films with a weight fraction of particles of 5 wt%. The number of samples for the measurements of as-prepared materials was $n \geq 4$, while the number of samples for materials, which had been immersed in SBF, was $n \geq 3$.
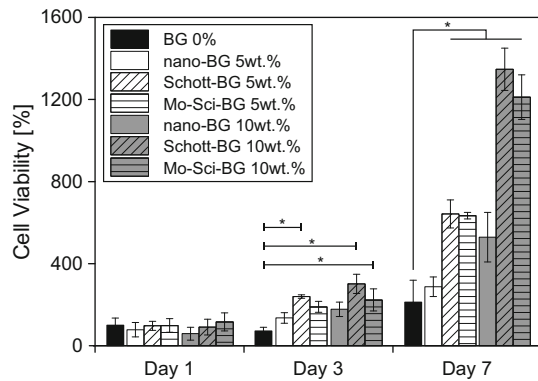
Figure 6 Cell proliferation of human primary dermal fibroblasts on different bioactive glass (BG45S5®) containing silicone composites. It shows the dependence of the cell viability on the particle type (nano-BG, Schott-BG and Mo-Sci-BG). The cell viabilities are compared to the one of day 1 on pure silicone. Positive control data are not shown, as it exceeded the viability of the best performing material by approximately 4-fold. * Significant differences for $p < 0.05$.

difference between Schott-BG and Mo-Sci-BG containing composites at the same compositions (5 wt%: $p = 0.09$; 10 wt%: $p = 0.50$; 15 wt%: $p = 0.42$). After immersion in SBF, the Young's modulus increased significantly for all particle-loaded samples compared to the value of the as-prepared composites ($p < 0.002$). The stiffness of pure silicone films did not change significantly after immersion in SBF ($p = 0.33$; Fig. 5f). 5 wt% nano-BG increased by a factor of two, while 10 wt% nano-BG increased by a factor of five. No systematic trend was found regarding a difference of Schott- and Mo-Sci-BG.

Cell culture study

Cell viability of primary human dermal fibroblasts did not differ significantly on BG containing silicone than on pure silicone after 24 h ($p = 1$; Fig. 6). After 3 days, the viabilities of the cells on 5 wt% ($p = 0.02$) and 10 wt% ($p = 0.0004$) Schott-BG and 10 wt% Mo-Sci-BG ($p = 0.04$) were significantly larger than on pure silicone on day 3. On day 3, only the viability on 10 wt% Schott-BG was significantly larger compared to other BG containing silicones (5 wt% nano-BG: $p = 7.3 \times 10^{-4}$ and 10 wt% nano-BG: $p = 0.02$). After 7 days, the viability of the cells on all BG-loaded silicones ($p \leq 2.8 \times 10^{-6}$) except 5 wt% nano-BG ($p = 1$) was significantly larger than on pure silicone on day 7. The viability on pure silicone did neither increase from day 1 to day 3 ($p = 1$), nor from day 3

to day 7 ($p = 0.11$). In general, the cell viability of human primary dermal fibroblasts was the largest on Schott-BG containing silicones, while it was larger on Mo-Sci-BG than on nano-BG-silicone composites.

Discussion

The here presented study examined the effect of different BG45S5® types (nano-BG, Schott-BG and Mo-Sci-BG) on medical grade silicone elastomers for the use at the driveline exit sites of left ventricular assist devices. As this position is specifically susceptible for infection, a stable polymer–skin interface is highly desirable, thus giving a barrier against pathogens [24]. Bioactive glass was chosen in this study, because of its reported wound healing properties and ability to improve the bioactivity of polymers [8, 12, 22, 35]. The experiments explored whether the simple incorporation of BG into silicone elastomers influences mechanical properties, improves bioactivity of silicone in body fluids and improves the silicone's cytocompatibility with human dermal cells. The use of different bioactive glasses enabled to study the influence of the particle size on the examined properties.

Incorporation of BG particles into silicone elastomers allowed the modification of mechanical and cytocompatibility properties of the polymer by pure mechanical mixing in an efficient way without the need for additional solvents or additives during production. Immersion of the silicone composites in simulated body fluid proved the HAp forming ability of the materials and thus its bioactivity. Improved cytocompatibility of primary human dermal fibroblasts with BG-filled silicone was proven. In the context of left ventricular assist device drivelines, the materials are suitable to cover the skin-penetrating driveline at the driveline exit site, improving the bioactivity and cytocompatibility compared to pure silicone.

Manufacturing

The manufacturing process was based on simple mechanical mixing and yielded well-distributed particles within the silicone matrix (Fig. 3). However, in contrast to the Schott-BG and Mo-Sci-BG microparticles, the production of films incorporating nano-BG particles at concentrations larger than

10 wt% was not possible, even at increased curing temperatures. The large surface area of nano-BG compared to the microparticles may result in large agglomerate formation, causing phase separation of the filler and the silicone and finally inhibiting the curing reaction due to the resulting large viscosity. Another explanation could be the inhibition of the platinum catalyst of the silicone elastomer caused by the nanoparticles. This has been reported earlier by Fahrni et al. [36] in a mixture of iron oxide nanoparticles in poly(dimethylsiloxane). Schrooten et al. [37] already reported the use of a BG coating with silicone rubber for percutaneous implants. They used electron beam ablation to coat poly(dimethyl-siloxane) with bioactive glass. However, the pure mechanical mixing reported here seems simpler and less technically demanding. As the particles can also be chemically defined prior to mixing into the uncured silicone, it is also possible to produce a more well-defined material, compared to the in situ formation of the BG with electron beam ablation.

Bioactivity

The in vitro study in SBF proved the formation of HAp and, thus, the bioactivity of BG containing silicone composites. The formation of HAp was confirmed visually by SEM (Fig. 3, Fig. S8), as well as by its crystal structure observed on XRD patterns with the characteristic signals at $2\Theta = 26°$ (0002) and $2\Theta = 31.5°$ (112) (Fig. 4c, d, Fig. S4-6). More HAp precipitated on nano-BG than on Schott-BG or Mo-Sci-BG containing silicone materials. This increased potential of nano-BG particles to form HAp was already reported earlier by Mačković et al. [38] and is attributed to the high surface reactivity of the nanoscale particles. Mačković et al. [38] also reported the formation of nanocrystalline HAp on nano-BG compared to BG microparticles. This could not be observed here as the peaks of HAp, formed on all BG containing composites seemed evenly broad, thus allowing no statements regarding HAp crystallite size. The formation of calcite on SBF-immersed Bioglass was already reported in earlier studies and is attributed to the mechanism of HAp formation in SBF [39, 40]. Larger surface areas of BG favour the release of calcium from BG, which increases the ratio of the calcium to phosphorous ions in solution (Ca/P ratio) [39, 40]. This causes the precipitation of calcite at the expense of HAp formation, which takes place in parallel in the first stages of BG reactions in SBF [38, 39]. Swelling of the composites in SBF was more prolonged for microparticles containing silicones than for nanocomposites. It suggests a reduced shape stability of the possibly implanted devices in the body, when microparticles are used.

Cytocompatibility

Human primary dermal fibroblasts were chosen for this study. Besides keratinocytes and dermal microvascular endothelial cells, they serve as a standard cell culture model to evaluate the interface between skin and percutaneous devices [41]. As the goal of this study was to gain a first evaluation, whether BG could serve as a material to improve the cytocompatibility at the skin of silicone elastomers, the study confined itself to the measurement of the fibroblast cell proliferation and the influence of different BG-silicone composites thereof. The results showed that BG containing silicone seems to allow a faster cell proliferation of human dermal fibroblasts than pure medical grade silicone. The slow proliferation of cells on pure silicone is attributed to the silicone elastomers' inertness and, thus, weak protein (Fig. S11) and cell attachment, which leads to weak soft tissue integration [42, 43]. The incorporation of BG into the silicone seems to allow a faster cell attachment of human dermal fibroblasts, which is a requirement for the proliferation of this cell type. This faster proliferation of the skin cells on the BG-silicone composites could allow faster wound closure between the implant and skin, thus forming a silicone–skin interface and a barrier against pathogens [22]. Once the dermal cells are able to proliferate on the polymer, faster skin biointegration of percutaneous materials is most likely. Also, the abilities of BG to support rapid wound closure has been shown earlier by Cai et al., who incorporated BG in an ointment and applied it to full thickness skin wounds in a rabbit model. They observed significantly shorter healing times with BG containing ointments compared to the control [35]. The combination of improved cell proliferation and reduced healing times makes BG a suitable material to improve the cytocompatibility of pure silicone and might therefore form an improved silicone–skin interface. However, the use of such BG containing silicones should not be considered for the use in other silicone elastomer containing implants, such as, e.g. breast implants. Here, silicone shell incrustation
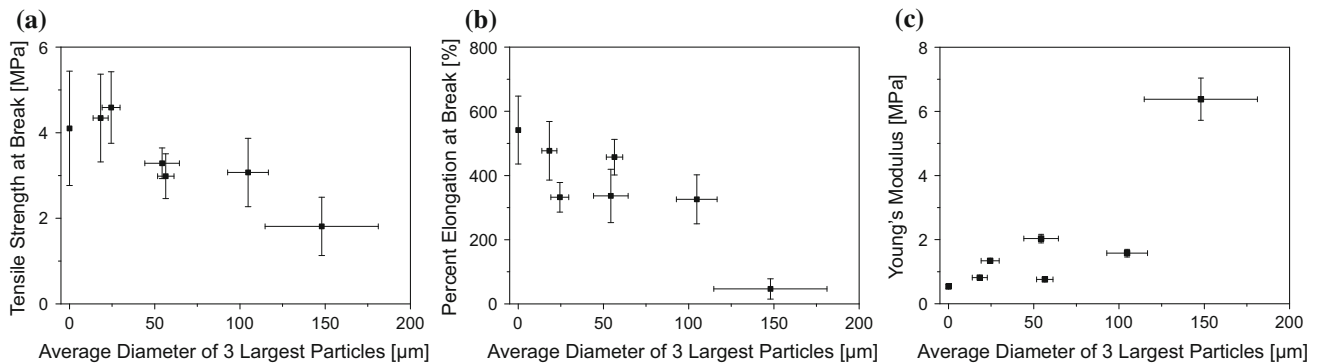
Figure 7 Tensile strength at break **a**, the percent elongation at break **b** and Young's modulus **c** of silicone films depending on the size of the largest particles or agglomerates, which are incorporated in silicone. In this analysis, the mean particle diameter of the three largest particles at the position of rupture was analysed. The films that include particles at a concentration of 10 wt% before and after immersion in simulated body fluid for 4 weeks and pure silicone were considered.

(calcification) is problematic, leading to stiffening and, in most dramatic cases implant rupture [44]. The use of BG containing silicones with LVADs would need to be limited to the driveline exit site. The measured cell viability and proliferation on BG containing silicones is limited compared to the surfaces of well plates and cell flasks but the comparison with pure medical grade silicone is promising. In addition, the increased cell viability on BG containing silicones after 7 days is indicative that this material allows the formation of a possibly stable connection to dermal cells. In general, the results allow to make an argument about the dependence of particle concentration of the silicone composite on the cell viability of the human dermal fibroblasts, which increases with particle concentration. Also microcomposites seem to promote cell proliferation better than nanocomposites. The reduced cell viability on the nano-BG containing silicones compared to Schott- and Mo-Sci-BG composites may be attributed to the increased alkalinity, induced by the dissolution of the BG particles [45]. As nano-BG exhibits larger specific surfaces, it increases the pH more than microparticles. The same applies to the viability on day 1. Due to the reaction of the BG with the cell medium, the alkalinity increased in the medium, which supposes a negative impact on the cell proliferation of fibroblasts. Still, also incorporated nano-BG increased the cell viability of cells compared to pure silicone and improved the cytocompatible properties thereof.

Mechanical properties

With exceptions, the results of the evaluation of the tensile strength at break and the percent elongation at break did not have statistical significance. The test method employed considers the tensile properties of thin plastic sheeting with a thickness of less than 1 mm. The test method also regards thin sheeting of elastomeric plastics with a percent elongation of larger than 100%, which justifies the choice of the test method. Despite the lack of significant results, the data still show general trends. Results were compared with the standard theories of ultimate strength and ultimate strain of particle-loaded polymer composites and tensile properties of human skin [46]. The latter is mainly defined by the properties of collagen, whose maximum strain is between 10 and 20%, while its maximum strength is approximately 70–150 MPa [47]. The tested silicone composites have larger values of ultimate strain, while the tensile strength at break is smaller than the one of collagen. The Young's modulus of the skin is between 0.42 MPa for young and 0.85 MPa for older humans [48]. Thus, the composites generally show larger elastic moduli, but smaller ultimate strength compared to human skin, when possibly implanted into the body. Under large forces, caused by possible accidents of the patient, the silicon–skin interface or the material could be compromised, depending on the strength of an eventually formed silicone–skin interface.

Ultimate mechanical properties

The tensile strength at break and percent elongation at break (other than the Young's modulus, which is measured for small strains) depend on the weakest path throughout the structure, as opposed to the statistically averaged values of the microstructure parameters [46]. Thus, the tensile strength at break and percent elongation at break are also defined by the size of the largest particles or largest discontinuity in the films, which defines the weakest point of the film (Fig. 7). The stress transfer under large strain is specifically weak at these positions, thus compromising the mechanical stability of the entire construct. The incorporation of particles generally decreased the ultimate tensile properties of the composites, which suggests weak particle–matrix interactions [49]. Before immersion in SBF, nano-BG and Schott-BG are well incorporated into the silicone, showing some particle/matrix interaction (Fig. 3b, c), while in the Mo-Sci-BG films, voids between silicone and particles can be observed (Fig. 3d). The stress transfer between the silicone and Mo-Sci particles is weak, thus, leading to the reduced ultimate tensile properties of Mo-Sci-BG-silicone composites. As the rather large Mo-Sci particles also possess sharp edges due to their shard-like nature, it is possible that these edges cut the silicone under stress and caused a rupture of the film. For the smaller particles of nano-BG and Schott-BG, the tensile strength at break is not influenced, even though the Schott-BG particles also show a shard-like morphology (Fig. 2b). This suggests that the stress transfer between particles and matrix is better for smaller particles [50]. The heavily decreased ultimate properties of the nano-BG composites compared to microparticles incorporating composites after immersion in SBF are probably due to the porosity of the nano-BG agglomerates, which are, besides much smaller aggregates, present in the matrix (Fig. 3b and Fig. S8b). This porosity yields a much larger specific surface area of the nano-BG compared to non-porous particles such as Schott-BG and Mo-Sci-BG, and thus, the nano-BG agglomerates have the aforementioned higher potential to form HAp [38]. This increased formation of HAp of the nano-BG particles in the silicone was also verified by XRD (Fig. 4). HAp formed on the internal pore walls of these nano-BG agglomerates causing an internal force within the agglomerate and, thus, weakening of the structure. Under strain, the agglomerate cracked from the inside, resulting in a large weak spot in the material. Figure 3e depicts one of the possible weak spots. These weaknesses could also be observed in light microscopy images (Fig. S7b) of the nano-BG-silicone films after immersion in SBF. As the ultimate mechanical properties are defined by the weakest path in the polymer, the weaknesses resulted in the destabilization of the entire film. Immersion in SBF also reduced the tensile strength at break of the Schott-BG containing composites, which can be explained by the reduced particle/matrix interactions caused by the formation of HAp on the surface of the particles. The reduced interactions resulted in voids between particles and silicone as seen in the cross-sectional SEM images (Fig. 3f), thus weakening the stress transfer under strain. Percent elongation at break was highly affected by the immersion in SBF for all particle types. This is due to the weak force transfer between particles and matrix after immersion in SBF, yielding the maximum stress of the composite at smaller strains.

Young's modulus

The incorporation of particles into a polymer causes a stiffening of the matrix because of the larger modulus of the solid particles [46]. Chen et al. [12] have shown this by incorporating flame spray synthesized nano-sized BG particles into poly(glycerol sebacat) (PGS). The main difference to this study lies in the hydrophobicity/hydrophilicity of the polymers and, thus, the particle/polymer interfacial adhesion. PGS has a similar hydrophilicity as collagen, while silicone is highly hydrophobic [11, 51, 52]. The results of the BG-silicone composites follow the same trend and coincide with the known literature [46]. The Young's modulus is generally not affected by the particle/matrix interactions because for small strains; there is insufficient dilation to cause interface separation [46]. Stiffness of silicone increased with addition of BG, indicating that no particle–matrix debonding occurred when samples were subject to tensile loading. The exaltation of the Young's modulus with increasing particle loading can be explained by the higher modulus of the particles compared to the silicone rubber. As a first approximation of this correlation of modulus and filler volume fraction, the equation of Guth can be used [53].

$$E_c/E_m = 1 + 2.5\, V_p + 14.1\, V_p^2$$

E_c and E_m are the Young's moduli of the composite and the matrix (pure silicone in this study), respectively. V_p is the particle volume fraction. Many other and more advanced equations for the description of the Young's modulus in relation to the volume fraction of the filler exist [46]. As indicated by the equation, higher volume fractions of inorganic fillers in the polymer result in a stiffer composite [46]. This is most probably also the explanation for the increased modulus of BG-silicone composites after immersion in SBF compared to the as-prepared films. As seen in the cross-sectional images of Fig. 3 and the light microscopy images of Fig. S7, the size of the incorporated BG particles is larger, which leads to an increase in volume fraction and, thus, causes the increased stiffness of the composites [46]. At same particle concentrations, the Young's modulus of Schott- and Mo-Sci-BG differs only slightly, while it is significantly higher for nano-BG ($p < 0.0005$). This increase in Young's modulus of nano-BG containing polymers compared to microparticles containing polymers was already reported earlier by Misra et al. [45] and is attributed to the true reinforcement achieved using nano-BG. The finer dispersed nanoparticles form crystalline HAp throughout the silicone matrix, thus causing the stiffening of the composite, while on the microparticles HAp only formers very localized at the particles.

Limitations of the study

The study is limited in several aspects. It cannot definitely predict, whether BG containing silicone are improving the driveline exit site of LVAD drivelines. Cell proliferation measurements of human skin cells (primary dermal fibroblasts) were conducted to assess the cytocompatibility of the material, but do not allow predictions about cell adhesion and long-term skin tissue integration. Mechanical testing showed results with large standard deviations. Some trends are visible, though mainly without statistical significance. Moreover, at increased sample sizes, it is improbable that standard deviations decrease, as this was tested for 5 wt% Mo-Sci-BG containing silicone with a samples size of 14. However, specifically the incorporation of nanosized particles is difficult at the presented concentrations. The static contact angle measurements also showed large errors and no significant results and trends could be observed. Still, as

for the mechanical testing, some minor trends are visible and increased sample sizes could improve the results.

Conclusion

Incorporation of nano-BG particles into silicone composites showed the highest bioactivity as measured by XRD and least swelling by 50%, but lower mechanical properties with an ultimate tensile strength of only 2 MPa after simulation of the environment in the human body and lower cytocompatibility. In contrast, micron sized particles were twice more cytocompatible than nanoparticles and had better mechanical properties and easier handling. Choosing the "right" particle type constitutes as a trade-off between different properties and will depend on the specific use. In the case of driveline material for LVAD implantation, the use of nano-sized BG45S5® would be more advantageous because of higher bioactivity and less swelling inside the body. In conclusion, this study served as a first evaluation, if BG containing silicone elastomers could be a suitable material for LVAD drivelines. The here presented mechanical properties and cytocompatibility are promising. Whether the materials meet the conditions for long-term implantation as a percutaneous driveline, especially with a focus on mechanical integrity, skin biointegration and reduced infection rates, has to be assessed in an animal model with the final LVAD driveline shape.

Compliance with ethical standards

Conflict of interest All authors declare no conflict of interest.

8) contains supplementary material, which is available to authorized users.

References

[1] Hench LL, Splinter RJ, Allen WC, Greenlee TK (1971) Bonding mechanisms at the interface of ceramic prosthetic materials. J Biomed Mater Res 5:117–141

[2] Hench LL (2006) The story of Bioglass®. J Mater Sci Mater Med 17:967–978

[3] Hench LL (1998) Bioceramics, a clinical success. Am Ceram Soc Bull 77:67–74

[4] Jones JR (2013) Review of bioactive glass: from Hench to hybrids. Acta Biomater 9:4457–4486

[5] Hoppe A, Güldal NS, Boccaccini AR (2011) A review of the biological response to ionic dissolution products from bioactive glasses and glass-ceramics. Biomaterials 32:2757–2774

[6] Xynos ID, Edgar AJ, Buttery LDK, Hench LL, Polak JM (2000) Ionic products of bioactive glass dissolution increase proliferation of human osteoblasts and induce insulin-like growth factor II mRNA Expression and protein synthesis. Biochem Biophys Res Commun 276:461–465

[7] Jell G, Stevens MM (2006) Gene activation by bioactive glasses. J Mater Sci Mater Med 17:997–1002

[8] Miguez-Pacheco V, Hench LL, Boccaccini AR (2015) Bioactive glasses beyond bone and teeth: emerging applications in contact with soft tissues. Acta Biomater 13:1–15

[9] Gorustovich AA, Roether JA, Boccaccini AR (2009) Effect of Bioactive glasses on angiogenesis: a review of in vitro and in vivo evidences. Tissue Eng Part B Rev 16:199–207

[10] Hu S, Chang J, Liu M, Ning C (2009) Study on antibacterial effect of 45S5 Bioglass®. J Mater Sci Mater Med 20:281–286

[11] Rai R, Tallawi M, Grigore A, Boccaccini AR (2012) Synthesis, properties and biomedical applications of poly(glycerol sebacate) (PGS): a review. Prog Polym Sci 37:1051–1078

[12] Chen Q, Jin L, Cook WD, Mohn D, Lagerqvist EL, Elliott DA, Haynes JM, Boyd N, Stark WJ, Pouton CW, Stanley EG, Elefanty AG (2010) Elastomeric nanocomposites as cell delivery vehicles and cardiac support devices. Soft Matter 6:4715–4726

[13] Ostomel TA, Shi Q, Tsung C-K, Liang H, Stucky GD (2006) Spherical bioactive glass with enhanced rates of hydroxyapatite deposition and hemostatic activity. Small 2:1261–1265

[14] Bunting S, Di Silvio L, Deb S, Hall S (2005) Bioresorbable glass fibres facilitate peripheral nerve regeneration. J Hand Surg Eur 30:242–247

[15] Boccaccini AR, Blaker JJ, Maquet V, Day RM, Jérôme R (2005) Preparation and characterisation of poly(lactide-co-glycolide) (PLGA) and PLGA/Bioglass® composite tubular foam scaffolds for tissue engineering applications. Mater Sci Eng C Mater Biol Appl 25:23–31

[16] Moosvi SR, Day RM (2009) Bioactive glass modulation of intestinal epithelial cell restitution. Acta Biomater 5:76–83

[17] Walker RD, Wilson J, Clark AE (1992) Injectable bioglass as a potential substitute for injectable polytetrafluoroethylene. J Urol 148:645–647

[18] Verrier S, Blaker JJ, Maquet V, Hench LL, Boccaccini AR (2004) PDLLA/Bioglass® composites for soft-tissue and hard-tissue engineering: an in vitro cell biology assessment. Biomaterials 25:3013–3021

[19] Hench LL, Greenspan D (2013) Interactions between bioactive glass and collagen: a review and new perspectives. J Aust Ceram Soc 49:1–40

[20] Marotta JS, LaTorre G, Batich C, Hench LL (2001) Percutaneous biofixed medical implants. US Patent US6299930 B1, Oct 9

[21] Ross EA, Batich CD, Clapp WL, Sallustio JE, Lee NC (2003) Tissue adhesion to bioactive glass-coated silicone tubing in a rat model of peritoneal dialysis catheters and catheter tunnels. Kidney Int 63:702–708

[22] Rai R, Roether JA, Knowles JC, Mordan N, Salih V, Locke IC, Gordge MP, Cormick AM, Mohn D, Stark WJ, Keshavarz T, Boccaccini AR, Roy I (2016) Highly elastomeric poly(3-hydroxyoctanoate) based natural polymer composite for enhanced keratinocyte regeneration. Int J Polym Mater Po 66:326–335

[23] McCandless SP, Ledford ID, Mason NO, Alharethi R, Rasmusson BY, Budge D, Stoker SL, Clayson SE, Doty JR, Thomsen GE, Caine WT, Kfoury AG, Reid BB, Miller DV (2015) Comparing velour versus silicone interfaces at the driveline exit site of HeartMate II devices: infection rates, histopathology, and ultrastructural aspects. Cardiovasc Pathol 24:71–75

[24] Dean D, Kallel F, Ewald GA, Tatooles A, Sheridan BC, Brewer RJ, Caldeira C, Farrar DJ, Akhter SA (2015) Reduction in driveline infection rates: results from the HeartMate II multicenter driveline silicone skin interface (SSI) registry. J Heart Lung Transplant 34:781–789

[25] von Recum AF, Park JB (1981) Permanent percutaneous devices. Crit Rev Bioeng 5:37–77

[26] Rubinfeld G, Levine JP, Reyentovich A, DeAnda A, Balsam LB (2015) Management of rapidly ascending driveline tunnel infection. J Card Surg 30:853–855

[27] Feldman DS, Hultman SM, Colaizzo RS, von Recum AF (1983) Electron microscope investigation of soft tissue

ingrowth into Dacron® velour with dogs. Biomaterials 4:105–111

[28] Merchel RA, Reid BB, McCandless SP, Caine WT, Ledford ID, Clayson SE, Carter AK, Rasmusson B, Stoker S, Budge D, Alharethi RA, Kfoury AG (2012) Impact of driveline material and size on exit site healing time in left ventricular assist devices. J Heart Lung Transplant 31:S21

[29] Ledford I, Miller D, Mason N, Alharethi R, Rasmusson B, Budge D, Stoker S, Clayson S, Doty J, Thomsen G (2011) 8 differential infection rates between velour versus silicone interface at the HeartMate II driveline exit site: structural and ultrastructural insight into possible causes. J Heart Lung Transplant 30:S10–S11

[30] Ledford ID, Miller DV, Mason NO (2011) Differential infection rates between velour versus silicone interface at the HeartMate II driveline exit site: structural and ultrastructural insight into possible causes. In: Paper presented at the International Society for Heart and Lung Transplantation, San Diego, CA, April 13–16

[31] Brunner TJ, Grass RN, Stark WJ (2006) Glass and bioglass nanopowders by flame synthesis. Chem Commun 13:1384–1386

[32] Kokubo T, Takadama H (2006) How useful is SBF in predicting in vivo bone bioactivity? Biomaterials 27:2907–2915

[33] Misra SK, Ansari TI, Valappil SP, Mohn D, Philip SE, Stark WJ, Roy I, Knowles JC, Salih V, Boccaccini AR (2010) Poly(3-hydroxybutyrate) multifunctional composite scaffolds for tissue engineering applications. Biomaterials 31:2806–2815

[34] Schneider OD, Loher S, Brunner TJ, Uebersax L, Simonet M, Grass RN, Merkle HP, Stark WJ (2008) Cotton wool-like nanocomposite biomaterials prepared by electrospinning: in vitro bioactivity and osteogenic differentiation of human mesenchymal stem cells. J Biomed Mater Res Part B 84B:350–362

[35] Lin C, Mao C, Zhang J, Li Y, Chen X (2012) Healing effect of bioactive glass ointment on full-thickness skin wounds. Biomed Mater 7:045017

[36] Fahrni F, Prins MWJ, van Ijzendoorn LJ (2009) Magnetization and actuation of polymeric microstructures with magnetic nanoparticles for application in microfluidics. J Magn Magn Mater 321:1843–1850

[37] Schrooten J, Jaecques SVN, Eloy R, Delubac C, Schultheiss C, Brenner P, Buth LHO, Van Humbeeck J, Sloten JV (2004) Bioactive glass coating for hard and soft tissue bonding on Ti6Al4V and silicone rubber using electron beam ablation. Key Eng Mater 254–256:427–430

[38] Mačković M, Hoppe A, Detsch R, Mohn D, Stark WJ, Spiecker E, Boccaccini AR (2012) Bioactive glass (type 45S5) nanoparticles: in vitro reactivity on nanoscale and biocompatibility. J Nanopart Res 14:1–22

[39] Jones JR, Sepulveda P, Hench LL (2001) Dose-dependent behavior of bioactive glass dissolution. J Biomed Mater Res 58:720–726

[40] Mozafari M, Moztarzadeh F, Tahriri M (2010) Investigation of the physico-chemical reactivity of a mesoporous bioactive SiO_2–CaO–P_2O_5 glass in simulated body fluid. J Non Cryst Solids 356:1470–1478

[41] Fukano Y, Knowles NG, Usui ML, Underwood RA, Hauch KD, Marshall AJ, Ratner BD, Giachelli C, Carter WG, Fleckman P, Olerud JE (2006) Characterization of an in vitro model for evaluating the interface between skin and percutaneous biomaterials. Wound Repair Regen 14:484–491

[42] Abbasi F, Mirzadeh H, Katbab A-A (2001) Modification of polysiloxane polymers for biomedical applications: a review. Polym Int 50:1279–1287

[43] Jarrell JD, Dolly B, Morgan JR (2010) Rapid screening, in vitro study of metal oxide and polymer hybrids as delivery coatings for improved soft-tissue integration of implants. J Biomed Mater Res A 92:1094–1104

[44] de Camara DL, Sheridan JM, Kammer BA (1993) Rupture and aging of silicone gel breast implants. Plast Reconstr Surg 91:828–834

[45] Misra SK, Mohn D, Brunner TJ, Stark WJ, Philip SE, Roy I, Salih V, Knowles JC, Boccaccini AR (2008) Comparison of nanoscale and microscale bioactive glass on the properties of P(3HB)/Bioglass® composites. Biomaterials 29:1750–1761

[46] Fu S-Y, Feng X-Q, Lauke B, Mai Y-W (2008) Effects of particle size, particle/matrix interface adhesion and particle loading on mechanical properties of particulate–polymer composites. Compos Part B Eng 39:933–961

[47] Meyers MA, Chen P, Lin AY, Seki Y (2008) Biological materials: structure and mechanical properteies. Prog Mater Sci 53:1–206

[48] Agache PG, Monneur C, Leveque JL, De Rigal J (1980) Mechanical properties and Young's modulus of human skin in vivo. Arch Dermatol Res 269:221–232

[49] Kemaloglu S, Ozkoc G, Aytac A (2010) Properties of thermally conductive micro and nano size boron nitride reinforced silicon rubber composites. Thermochim Acta 499:40–47

[50] Landon G, Lewis G, Boden GF (1977) The influence of particle size on the tensile strength of particulate—filled polymers. J Mater Sci 12:1605–1613. doi:10.1007/BF00542811

[51] Wang Y, Ameer GA, Sheppard BJ, Langer R (2002) A tough biodegradable elastomer. Nat Biotechnol 20:602–606

[52] Dupont-Gillain CC, Nysten B, Rouxhet PG (1999) Collagen adsorption on poly(methyl methacrylate): net-like structure formation upon drying. Polym Int 48:271–276

[53] Guth E (1945) Theory of filler reinforcement. J Appl Phys 16:20–25